Atmos. Chem. Phys. Discuss., 9, 18113–18158, 2009
www.atmos-chem-phys-discuss.net/9/18113/2009/

Atmospheric Chemistry and Physics Discussions

This discussion paper is/has been under review for the journal *Atmospheric Chemistry and Physics (ACP)*. Please refer to the corresponding final paper in *ACP* if available.

Characterization of a large biogenic secondary organic aerosol event from eastern Canadian forests

J. G. Slowik[1], C. Stroud[2], J. W. Bottenheim[2], P. C. Brickell[2], R. Y.-W. Chang[1], J. Liggio[2], P. A. Makar[2], R. V. Martin[3,4], M. D. Moran[2], N. C. Shantz[1,2], S. J. Sjostedt[1], A. van Donkelaar[3], A. Vlasenko[1,2], H. A. Wiebe[2], A. G. Xia[2], J. Zhang[2], W. R. Leaitch[2], and J. P. D. Abbatt[1]

[1]University of Toronto, Department of Chemistry, Toronto, ON, Canada
[2]Environment Canada, Science and Technology Branch, Toronto, ON, Canada
[3]Dalhousie University, Department of Physics and Atmospheric Science, Halifax, NS, Canada
[4]Harvard-Smithsonian Center for Astrophysics, Atomic and Molecular Physics Division, Cambridge, MA, USA

Received: 3 July 2009 – Accepted: 8 August 2009 – Published: 1 September 2009

Correspondence to: J. G. Slowik (jslowik@chem.utoronto.ca)

Published by Copernicus Publications on behalf of the European Geosciences Union.

Abstract

Biogenic secondary organic aerosol levels many times larger than past observations have been measured 70 km north of Toronto during a period of increasing temperatures and outflow from Northern Ontario and Quebec forests in early summer. A regional chemical transport model approximately predicts the event timing and accurately predicts the aerosol loading, identifying the precursors as monoterpene emissions from the coniferous forest. The agreement between the measured and modeled biogenic aerosol concentrations contrasts with model underpredictions for polluted regions. Correlations of the oxygenated organic aerosol mass with tracers such as CO support a secondary aerosol source and distinguish biogenic, pollution, and biomass burning periods during the field campaign. Using the Master Chemical Mechanism, it is shown that the levels of CO observed during the biogenic event are consistent with a photochemical source arising from monoterpene oxidation. The biogenic aerosol mass correlates with satellite measurements of regional aerosol optical depth, indicating that the event extends across the eastern Canadian forest. This regional event correlates with increased temperatures, indicating that temperature-dependent forest emissions can significantly affect climate through enhanced direct radiative forcing and higher cloud condensation nuclei numbers.

1 Introduction

There has been intense interest of late in the nature of the organic component of the tropospheric aerosol, specifically its complex composition, oxidation state, hygroscopicity, and reactivity. While a number of secondary organic aerosol (SOA) formation routes have been presented, there remain considerable uncertainties in determining the most significant pathways by which organic mass accumulates on tropospheric particles (Goldstein and Galbally, 2007; Hallquist et al., 2009; Kanakidou et al., 2005). The conventional perspective has been that reactive volatile organic compounds (VOCs)

ACPD

9, 18113–18158, 2009

from biogenic emissions (e.g. monoterpenes and, more recently, isoprene) or anthropogenic sources (e.g. aromatic hydrocarbons) are oxidized to form less volatile products that then partition to particles. Comparisons of observed and modeled organic aerosol loadings have been examined in case studies of urban areas (Dzepina et al., 2009; Volkamer et al., 2006) and urban outflow, yielding a systematic underprediction by models that increases with photochemical age (de Gouw et al., 2008; Johnson et al., 2006; Volkamer et al., 2006). Biogenic SOA has been only addressed of late, in part because of the high amounts of organic aerosol observed during anthropogenic source studies. Most previous biogenic studies have observed significantly lower levels (Capes et al., 2009; Claeys et al., 2004; Gunthe et al., 2009; Kavouras et al., 1998; Tunved et al., 2006), despite studies indicating that global VOC emissions are higher from biogenic sources (Guenther et al., 2000, 1996).

However, some evidence exists that the biogenic SOA mass may be larger than previously observed. Higher biogenic SOA concentrations than those discussed above have been observed in a region of high terpene emissions (Shantz et al., 2004). Organic concentrations of 5.7 and 3.1 $\mu g/m^3$ were observed in eastern Canada during periods influenced by isoprene and monoterpene oxidation, respectively (Williams et al., 2007). However, the biogenic SOA mass fraction during these episodes is unknown. The interaction of biogenic VOCs with anthropogenic pollutants is hypothesized to contribute to high aerosol loadings in the southeast United States (Goldstein et al., 2009). Further, carbon isotope measurements suggest recent involvement in photosynthesis for the majority of organic aerosol carbon in a variety of settings, including polluted cases (Szidat et al., 2004; Weber et al., 2007). This finding makes comprehensive studies of biogenic aerosol formation events of extreme importance, to delineate the conditions under which biogenic aerosol readily forms and to describe the photochemical state of the atmosphere that is associated with such activity.

Here we present evidence for the formation of the most substantial biogenic organic aerosol formation event yet observed, from measurements at a rural location north of Toronto, Canada. The five day event is characterized by steadily increasing organic

ACPD
9, 18113–18158, 2009

aerosol levels to a maximum of 15 μg m^{-3}, correlated strongly with increasing temperature. Atmospheric CO levels increase concurrently. Wind flow was from the largely unpopulated regions of northern and central Ontario and Quebec. Through both in situ observations and regional air quality modeling results, the organic aerosol is shown to be photochemically produced from biogenic precursors. The increasing levels of CO are consistent with a photochemical source as well. Satellite observations of aerosol optical depth (AOD) highlight the importance of these forested areas as major aerosol source regions that will affect climate, the regional ecology, and air quality.

2 Materials and methods

2.1 Sampling location

Sampling for the Egbert 2007 field campaign was conducted from 14 May to 15 June 2007, at the Center for Atmospheric Research Experiments (CARE) in Egbert, Ontario, Canada (44.23 N, 79.78 W; 251 m above sea level). The Egbert CARE site is a permanent research station operated by Environment Canada. Egbert is a rural location consisting of mixed forest and farmland, approximately 70 km north of Toronto. Toronto is one of the largest urban areas in North America, with a population of 5 million, while the population of the Southern Ontario region is approximately 8 million. During periods of southerly winds, Egbert is influenced by the urban outflow of Toronto. In contrast, northerly winds bring air from sparsely populated, heavily forested regions. The only major anthropogenic sources to the north are from nickel and copper mining industries in the city of Sudbury (~300 km to the north).

ACPD
9, 18113–18158, 2009

2.2 Instrumentation

2.2.1 Aerosol mass spectrometer

The size-resolved, non-refractory composition of submicron aerosol particles was measured with an Aerodyne time-of-flight aerosol mass spectrometer (C-ToF-AMS) (Aerodyne Research, Inc., Billerica, MA, USA), which is described in detail in the literature (Canagaratna et al., 2007; Drewnick et al., 2005; Jayne et al., 2000; Jimenez et al., 2003). In brief, particles are sampled through a 100 μm critical orifice (2 torr) and passed through an aerodynamic lens. The lens both focuses the particles into a narrow beam and accelerates them to a velocity dependent on particle vacuum aerodynamic diameter (d_{va}). The particles impact a resistively heated surface (600°C, 10^{-7} torr) and flash-vaporize. The resulting gas is ionized by electron impact (70 eV) and the ions are detected by a time-of-flight mass spectrometer. The AMS may be operated in one of two modes: (1) The particle beam is alternately blocked and unblocked, yielding a full mass spectrum; or (2) The particle beam is modulated with a spinning chopper wheel (150 Hz), allowing determination of d_{va} from the particle time-of-flight between the chopper and detector. Because the mass spectrometer records spectra at 50 kHz, size-resolved mass spectra are obtained. The AMS used in this study was equipped with an optical scattering module, which provides a scattered light pulse for every particle impacting the vaporizer (Cross et al., 2007) above the optical detection limit of ~215 nm (geometric diameter). Incorporation of this module into the ToF-AMS enables the quantitative detection of single particle mass spectra (Cross et al., 2008). Data presented in the manuscript body are taken exclusively from ensemble mass spectra (5 min average), however the size-resolved and single particle spectra are used to evaluate the instrument collection efficiency, as discussed below.

An important consideration in the quantitative analysis of AMS data is the collection efficiency due to particle bounce (E_b). On impacting the vaporizer, some fraction of non-refractory particles bounces off the vaporizer surface instead of vaporizing. The detected number fraction is defined as the bounce collection efficiency (E_b), which

ACPD
9, 18113–18158, 2009

depends primarily on particle phase (Matthew et al., 2008). Typically E_b ~0.5 for ambient particles, although higher values have been obtained for acidic particles, particles with a high mass fraction of ammonium nitrate or liquid organics, and particles sampled at high relative humidity. Two methods were used to estimate E_b: (1) correlated optical scattering measurements and single particle mass spectra and (2) comparison of AMS and SMPS data. The two methods are described in more detail below. They yielded similar results and E_b was estimated to be 0.6.

E_b has traditionally been estimated through comparisons with co-located instrumentation. However, the combination of the optical scattering module and single particle mass spectra provides a direct in situ measurement of E_b as the fraction of light scattering pulses that contain a correlated chemical ion signal for particles larger than the 215 nm detection limit (Cross et al., 2008). We assume that the measured E_b for this particle subset extends across the entire size range to obtain a global estimate of E_b.

A second estimate of E_b was obtained through comparison of the AMS mass distributions with volume distributions from a scanning mobility particle sizer (SMPS) (differential mobility analyzer (DMA) model 3071 coupled to a condensation particle counter (CPC) model 3010, TSI, Inc., St. Paul, MN, USA), which measured mobility size distributions on a 15 min time interval for particles with mobility diameters (d_m) below 400 nm. AMS distributions were converted from mass to volume using the relationship $d_{va}=d_m \cdot \frac{\rho_p}{\rho_0} \cdot \frac{1}{\chi^2}$, where d_m is the SMPS-measured mobility diameter, ρ_p and ρ_0 are the particle and unit densities, respectively, and χ is the dynamic shape factor. We assumed spherical particles (i.e. χ=1) and component densities of 1.77 g cm^{-3} for sulfate, 1.74 g cm^{-3} for nitrate, 1.527 g cm^{-3} for chloride, a weighted average of the sulfate and nitrate densities for ammonium, and 1.2 g cm^{-3} for organics. The particle density and AMS cutpoint corresponding to d_m=400 nm were calculated independently for each 15 min interval.

In this manuscript, we report the semiquantitative AMS time series of potassium, measured at *m/z* 39. Because previous studies using the high-resolution VW-ToF-AMS have shown the *m/z* 39 signal to be dominated by $C_3H_3^+$ (Aiken et al., 2009), a further

description of this measurement is required. Although the C-ToF-AMS is primarily a unit resolution mass spectrometer, in the present study sufficient resolution exists to distinguish the signals at K^+ (*m/z* 38.963707) and $C_3H_3^+$ (*m/z* 39.023475) as discussed in the Supplement: (see Figs. S1–S5) http://www.atmos-chem-phys-discuss.net/9/18113/2009/acpd-9-18113-2009-supplement.pdf. Spectra were analyzed using the PIKA v1.06A software (D. Sueper, U. of Colorado-Boulder, USA) (DeCarlo et al., 2006). The time series of K^+ and $C_3H_3^+$ are presented in the Supplement (Fig. S1): http://www.atmos-chem-phys-discuss.net/9/18113/2009/acpd-9-18113-2009-supplement.pdf. A relative ionization efficiency (RIE) of 10 was estimated for potassium from calibration with KNO_3 (where RIE is defined in reference to the signal at *m/z* 30 and 46 for NO_3). This value is notably higher than a previously reported potassium RIE=2.9 (Drewnick et al., 2006). However, significant variation between instruments is expected to due to the effects of mass spectrometer tuning on the sampling efficiency of ions from surface ionization. The potassium measurement presented here should be considered only semi-quantitative due to (1) the low mass resolution of the C-ToF, (2) the high instrument background at *m/z* 39, and (3) competition between multiple ionization processes.

2.2.2 Cloud condensation nucleus counter

Cloud condensation nuclei (CCN) concentrations were measured using a home-built CCN counter (Kumar et al., 2003) consisting of a coupled continuous flow thermal gradient diffusion chamber (TGDC) and aerodynamic particle sizer (APS) model 3320 (TSI, Inc., St. Paul, MN, USA). The chamber supersaturation was calibrated using size-selected $(NH_4)_2SO_4$ particles and was set at 0.42% for the present experiments. CCN number concentrations are measured to within ±25%. Further details of instrument calibration, performance, and operation are available in the literature (Chang et al., 2007; Kumar et al., 2003).

ACPD
9, 18113–18158, 2009

2.2.3 Gas measurements

Volatile organic compounds (VOCs) were measured using a proton-transfer reaction mass spectrometer (PTR-MS) (de Gouw and Warneke, 2007; Lindinger et al., 1998) (Ionicon Analytik, Innsbruck, Austria) and a gas chromatography system coupled to a flame ionization detector system (GC-FID) (Brickell et al., 2003; Rupakheti et al., 2005). In the PTR-MS, H_3O^+ ions are generated by a cathode discharge in water vapor and ionize trace gases that have a higher proton affinity than water. The resulting ions are detected with a quadrupole mass spectrometer. Because this soft ionization technique causes relatively little fragmentation, measured *m/z*'s can frequently be directly related to the parent ion, and VOCs identified. The PTR-MS was calibrated with a custom standard containing 12 VOC species (methanol, acetonitrile, acetone, isoprene, methyl vinyl ketone, benzene, toluene, acetaldehyde, dimethylsulfide, α-pinene, limonene, 2-methyl-3-buten-2-ol) in the 500 ppbv range (Apel-Riemer Environmental Inc., Broomfield, CO, USA). Species-dependent calibration factors and detection limits are described elsewhere (Vlasenko et al., 2009). The GC-FID system employs a liquid nitrogen-cooled glass bead pre-concentration trap and multi-column capillary chromatography system. The instrument has detection limits of 5–16 pptv in an air sampling volume of 930 mL and was validated in a recent intercomparison study (Rappenglück et al., 2006). Gaseous CO and NO_x were measured using a TECO 48C and TECO 42C, respectively (Thermo Electron Corporation, Waltham, MA, USA).

2.3 Positive matrix factorization (PMF)

The AMS organic mass spectra were analyzed using positive matrix factorization (PMF) (Paatero, 1997; Paatero and Tapper, 1994), a receptor modeling technique that uses multivariate statistical methods to represent the time series of mass spectra as a linear combination of factor mass spectra and their time-dependent intensities. PMF analysis was performed using the PMF2 software package (P. Paatero, U. of Helsinki, Finland), together with the CU AMS PMF Tool (Ulbrich et al., 2009a). The PMF model

ACPD
9, 18113–18158, 2009

is described by the matrix equation:

$$\mathbf{X}=\mathbf{GF}+\mathbf{E} \quad (1)$$

Here **X** is the input mass spectral time series, the columns of the **G** matrix contain the factor time series and the rows of the **F** matrix contain the factor mass spectra. The **E** matrix contains the residuals and is defined by Eq. (1). The PMF model solves Eq. (1) by using a weighted least-squares algorithm to minimize the quantity Q, defined as:

$$Q=\sum_i \sum_j \left(e_{ij}/s_{ij}\right)^2 \quad (2)$$

Here e_{ij} are the elements of the residual matrix **E**, and s_{ij} are the elements of the uncertainty matrix **S**. The theoretical value of Q, denoted Q_{expected}, can be estimated as the number of elements in the input matrix **X**. In practice, Q is expected to be somewhat larger than Q_{expected} for ambient data because the data cannot be perfectly represented by a finite number of factors.

The AMS uncertainties (s_{ij}) discussed in Eq. (2) are calculated from the convolution of a Poisson distribution representing ion counting statistics with a detector-dependent Gaussian distribution representing the variation in single ion signal intensity (Allan et al., 2003). Uncertainties are calculated independently for the background and particle beam and summed in quadrature, yielding the expression $\Delta I_d=\alpha\frac{\sqrt{I_o+I_b}}{\sqrt{t_s}}$. Here I_o and I_b are the ion signals in the unblocked and blocked (background) positions, t_s is the sampling time, and α is a factor accounting for the width of the Gaussian distribution discussed above. The elements of the uncertainty matrix **S** are the ΔI_d values for each individual *m/z* at every point in time.

The PMF2 software was applied to a mass spectral matrix consisting of the organic component of all *m/z*'s ≤300, yielding a mass spectral matrix of 270 m/z's and 8143 mass spectra (not all *m/z*'s contain organic signal). The PMF2 "robust" operating mode was utilized, in which data points yielding large residuals ($|e_{ij}/s_{ij}|>4$) are iteratively downweighted (Paatero, 1997). Matrix rotations were explored by varying the *f*Peak

ACPD
9, 18113–18158, 2009

parameter from −1.5 to 1.5 (see Fig. S6: http://www.atmos-chem-phys-discuss.net/9/18113/2009/acpd-9-18113-2009-supplement.pdf) and provided results consistent with those presented below (obtained at *f*Peak=0.0). The possibility of local minima in the solution space was considered by initiating the PMF2 routine from 100 random starting points, denoted by seed values from 1 to 100. The different seed values yielded similar solutions to those presented below (obtained at seed=1), indicating that other local minima were not found (see Fig. S8: http://www.atmos-chem-phys-discuss.net/9/18113/2009/acpd-9-18113-2009-supplement.pdf). Selection of the correct number of factors, as well as factor identification, is discussed in Sect. 3.1.1.

2.4 AURAMS (A Unified Regional Air-quality Monitoring System) model

AURAMS (version 1.4.0) is an off-line chemical transport model (CTM) that is driven by the Canadian operational weather forecast model, GEM (Global Environmental Multi-scale model) (Côté et al., 1998a, b). GEM (version 3.2.2) was used to produce meteorological fields with a 15-km horizontal resolution. GEM was run for 12-h periods from reanalysis files with a 6-h spin-up and 6 h of simulation stored for the CTM. AURAMS was run in a one-way nested configuration with a continental-scale outer domain at 42-km resolution and an inner regional domain at 15-km resolution.

Hourly anthropogenic point, area, and mobile emission files were prepared for the CTM using the 2005 Canadian and 2005 US emissions inventories and version 2.3 of the SMOKE emissions processing system (CEP, 2003; Houyoux et al., 2000). Biogenic emissions were calculated on-line by AURAMS using BEIS version 3.09, the Biogenic Emissions Landcover Database (BELD3) vegetation data set (30 tree species and 20 crop species used for Canada), and meteorological fields (temperature and irradiance) from GEM. Biogenic VOC emissions are speciated into four groups: isoprene (ISOP), monoterpenes (PINE), sesquiterpenes (SESQ) and "other VOCs". Sesquiterpene emissions were calculated by scaling monoterpene emissions (Helmig et al., 2007) (e.g. SESQ emissions were a factor of 0.16 lower than monoterpenes at 30°C).

The gas-phase mechanism in AURAMS is an updated version of the ADOM-II mechanism (Kuhn et al., 1998), which is solved using a vectorized version of the rodas3 solver (Sandu and Sander, 2006). A detailed description of the ADOM-II VOC lumping scheme is presented elsewhere (Stroud et al., 2008). In the present study, a lumped monoterpene species was separated from the original ADOM-II anthropogenic long-chain alkene species and assigned the $OH/O_3/NO_3$ kinetics of α-pinene. A lumped sesquiterpene species was added to the mechanism and modeled with β-caryophyllene+O_3/OH/NO_3 kinetics. Benzene was separated from the original ADOM-II lumped species (sum of propane, acetylene, and benzene), and reacted in the modified mechanism with OH kinetics. The overall organic aerosol yield approach (Odum et al., 1996) was applied to the following VOC precursor species: isoprene (ISOP), monoterpenes (PINE), sesquiterpenes (SESQ), benzene (BENZ), mono-substituted aromatics (TOLU), multi-substituted aromatics (AROM), long chain anthropogenic alkenes (ALKE), and long chain anthropogenic alkanes (ALKA). Aerosol yields were calculated for low and high NO_x limits as a function of existing organic aerosol loadings (including both primary and secondary aerosol) and temperature. Updated α_i and K_i based on recent literature studies were applied for ISOP Kroll et al., 2006; Lane et al., 2008), PINE (Griffin et al., 1999; Pathak et al., 2007; Zhang et al., 2006), SESQ, ALKE, and ALKA (Lane et al., 2008), BENZ and AROM (Ng et al., 2007), and TOLU (Hildebrandt et al., 2009). An incremental increase in SOA mass was calculated from decreases in precursor VOC concentrations for a given time step under both low and high NO_x conditions. A linear interpolation between the low NO_x and high NO_x incremental SOA mass was performed based on the fraction of the RO_2 radicals which react with HO_x vs. NO_x (Henze et al., 2008; Presto and Donahue, 2006).

An organic particle density of 1.5 g cm^{-3} was assumed for conversion of normalized aerosol yield data (from particle volume measurements). The particle size distribution is represented in the CTM by 12 bins ranging in diameter from 0.01 to 40.96 μm, with the 8 lower bins corresponding to sizes below 2.5 μm. Particle composition is represented by nine species (sulfate, nitrate, ammonium, black carbon, primary organic

ACPD
9, 18113–18158, 2009

aerosol, SOA, crustal material, sea salt, and particulate water), which are assumed to be internally mixed within each size bin (Smyth et al., 2009). Condensation of the SOA to the particle size distribution is described by a modified Fuchs-Sutugin equation as described by equation A14 in Gong et al. (2003).

2.5 Moderate Resolution Imaging Spectroradiometer (MODIS) remote sensing

The spatial and temporal domain of this analysis is extended using satellite observations from the Moderate Resolution Imaging Spectroradiometer (MODIS) onboard the Terra satellite. MODIS/Terra has taken global daily measurements of solar backscatter at 10:30 AM local time since mid-2000. The retrieval of aerosol optical depth (AOD), a measure of light extinction by aerosol in the atmospheric column, is described in the literature (Levy et al., 2007; Remer et al., 2005). Validation of the retrieved AOD with ground-based AERONET observations yields a typical accuracy of 0.05±15% (Remer et al., 2005). We use here Collection 5 level 2 quality 3 data. The MODIS fire count algorithm, available from the USDA Forest Service, Remote Sensing Applications Center, uses brightness temperature from the MODIS 4 μm and 11 μm channel to detect the presence of fire (Giglio et al., 2003).

3 Results and discussion

3.1 AMS organic mass spectral analysis

3.1.1 Positive Matrix Factorization (PMF)

The application of PMF to an AMS dataset has been previously described in detail (Lanz et al., 2007; Slowik et al., 2009; Ulbrich et al., 2009a). An important consideration is the number of factors output by the PMF algorithm, which is selected by the user. However, no completely unambiguous method for choosing the "correct" number of factors exists. The selected number of factors is thus somewhat subjective and must

ACPD
9, 18113–18158, 2009

be validated through comparisons of factor and tracer time series, analysis of the factor mass spectra, and the evolution of the residual time series as a function of the number of resolved factors. Here a 4-factor solution was selected as the best representation of the data, as described below.

In Fig. 1, we plot the time series of the quantity $\Delta\left(\sum_j \left(e_{ij}/s_{ij}\right)^2\right)$ between two solutions with different numbers of factors: that is, the time-dependent contribution to Q for the n-factor solution minus that of the (n+1)-factor solution. The appearance of time series structure in such a plot indicates that the increased number of factors enables more of the data to be explained. Structure is evident in Fig. 1a–c, but is substantially reduced in Fig. 1d. (Note that the scale in Fig. 1a is ~60x that of Fig. 1b and ~120x that of Fig. 1c and d.) These trends in time series structure indicate that the PMF solution is enhanced by increasing the number of factors to 4, but that further improvements do not explain significantly more of the data.

As described below, the 4-factor solution contains factors identified as hydrocarbon-like organic aerosol (HOA), biomass burning organic aerosol (BBOA), and more- and less-oxygenated organic aerosol (denoted as OOA-1 and OOA-2, respectively), designations that result from correlations with tracer species and comparison with previous PMF analyses of AMS data, as discussed below. Increasing the number of factors to 5 yields a third OOA factor and alters the mass spectra and time series of the OOA-1 and OOA-2 factors (see Fig. S6: http://www.atmos-chem-phys-discuss.net/9/18113/2009/acpd-9-18113-2009-supplement.pdf). This is consistent with factor mixing/splitting behavior, previously identified as an indicator of an excessive number of factors (Ulbrich et al., 2009a). Further, the additional OOA factor does not aid the interpretation of the dataset. Therefore, the 4-factor solution was selected.

ACPD
9, 18113–18158, 2009

3.1.2 Validation and analysis of AMS PMF factors

The factor mass spectra and time series for the 4-factor PMF solution are plotted in Fig. 2. Figure 2b also shows the time series of tracer species correlated with the PMF factors. Factor mass spectra are normalized such that the sum of each spectrum across all *m/z* is equal to 1. The factor time series are reported in units of mass concentration ($\mu g\,m^{-3}$). A brief discussion of the factor mass spectra and time series is presented below. All comparisons with previously reported spectra were performed using spectra obtained from the AMS Spectral Database (Ulbrich et al., 2009b).

The mass spectrum of the HOA factor (F1) correlates with that of HOA factors obtained in other locations (e.g. R^2=0.78 vs. Pittsburgh HOA (Zhang et al., 2005), R^2=0.54 vs. Zurich summer HOA (Lanz et al., 2007), and R^2=0.68 vs. Zurich winter HOA (Lanz et al., 2008)). The primary difference between the previously reported HOA spectra and Egbert HOA is that the Egbert HOA has more signal at low *m/z*'s, particularly *m/z* 15, 27, and 29. These three *m/z*'s comprise 15.3% of the spectrum vs. 4.4% to 7.8% in previous studies. Similar to previous studies, the HOA time series correlates with tracers of primary anthropogenic emissions, such as NO_x (R^2=0.41) and benzene (R^2=0.43) as shown in Fig. 2b.

The BBOA factor mass spectrum (Fig. 2a) is the only resolved factor containing significant signal at *m/z* 60 and 73. These fragments are characteristic of levoglucosan, a tracer for cellulose pyrolysis. The BBOA mass spectrum correlates both with that of levoglucosan (Schneider et al., 2006) (R^2=0.70) and a Zurich wood-burning PMF factor (Lanz et al., 2007) (R^2=0.80). In Fig. 2b, the BBOA time series is plotted together with the semi-quantitative AMS measurement of potassium (R^2=0.30) and PTR-MS measurement of acetonitrile (R^2=0.34).

The mass spectrum and time series of the more oxygenated OOA factor, denoted "OOA-1", are shown in Fig. 2a and b, respectively. Relative oxygenation is inferred from the ratio of *m/z* 44 (CO_2^+ ion) to the total mass spectrum. For OOA-1, the 44/total ratio is 0.19 (vs. 0.10 for the less oxygenated OOA-2). These values correspond to O/C

ACPD
9, 18113–18158, 2009

ratios of ∼0.81 (OOA-1) and ∼0.46 (OOA-2) based on the approximation presented by Aiken et al. (2008). Increased oxygenation is expected to correlate with increased particle age (Aiken et al., 2008; Lanz et al., 2007; Ulbrich et al., 2009a) and decreased volatility (Huffman et al., 2009). The OOA-1 mass spectrum closely resembles that of OOA factors extracted from AMS measurements in several locations (e.g. R^2=0.88 with vs. Pittsburgh OOA (Zhang et al., 2005)). As shown in Fig. 2b, the time series of OOA-1 correlates with AMS measurements of particulate sulfate (R^2=0.77), which is mostly attributed to long-range transport, and with acetone (R^2=0.70), a long-lived oxygenated VOC generated in part through photochemical reactions (Vlasenko et al., 2009).

Unlike the OOA-2 factors previously extracted from AMS datasets in Zurich and Pittsburgh (Lanz et al., 2007; Ulbrich et al., 2009a) where volatility is thought to drive the factor time series, Egbert OOA-2 does not correlate with particulate nitrate (not shown). Instead, Egbert OOA-2 correlates with VOC photochemical products. This is shown in Fig. 2b, where the OOA-2 time series is plotted together with that of PTR-MS *m/z* 71, which is attributed to methacrolein (MACR) and methyl vinyl ketone (MVK). These VOCs are photochemically generated and have lifetimes on the order of half a day (Biesenthal et al., 1998). OOA-2 also correlates with acetic acid (at PTR-MS *m/z* 61), a longer-lived product of VOC oxidation. Similar correlations are also observed with formaldehyde, acetone, and a factor obtained from PMF analysis of the PTR-MS spectrum (Vlasenko et al., 2009). In addition to the species already mentioned, the PTR-MS PMF factor includes the majority of the signal assigned to *m/z* 99 (pinonaldehyde fragment), *m/z* 113 (attributed to monoterpene oxidation products in chamber studies) (Lee et al., 2006a, b), and a number of other peaks expected to correspond with oxygenated compounds.

The relative age of the OOA-1 and OOA-2 factors can be inferred through the correlations of these factors with VOCs having known atmospheric lifetimes. Figure 3 shows the R^2 values for correlations of OOA-1 and OOA-2 with acetone, acetic acid, MACR+MVK, toluene, and monoterpenes over the entire study period. As expected,

ACPD
9, 18113–18158, 2009

neither factor correlates with toluene and monoterpenes. Both factors correlate with acetone, acetic acid, and MACR+MVK. However, OOA-2 correlates more strongly with MACR+MVK (lifetime of approximately half a day (Biesenthal et al., 1998)) than does OOA-1. In contrast, OOA-1 correlates more strongly with the longer-lived acetone and acetic acid (lifetime of days to weeks) than does OOA-2. The trends in these correlations indicate that (1) OOA-2 results from more recent oxidation than OOA-1, and (2) a large fraction of OOA-2 is formed within half a day (i.e. before MACR+MVK is destroyed).

3.2 Identification and characterization of the biogenic period

Figure 4 shows the time series of measured particulate inorganic species, organic factors from the PMF analysis, and selected VOCs. The dashed backgrounds denote periods selected for contrasting studies of biogenic influences, urban outflow, and biomass burning.

The biogenic period (9 June to mid-day on 13 June) corresponds with steadily increasing temperatures under clear sky conditions, with back trajectories (presented later in Fig. 10c) and surface wind direction indicating air transported from north of the site. During this period, the organic aerosol mass builds steadily, with local maxima in the afternoons of 11, 12, and 13 June. A corresponding increase is evident in the photochemical reaction products MACR and MVK. Acetylene (a long-lived anthropogenic tracer) mixing ratios remain very low. This behavior contrasts sharply with the elevated acetylene mixing ratios observed during periods of urban outflow from the south (e.g. 30 May to 4 June). Monoterpene mixing ratios are elevated during the 9 to 13 June period; however, monoterpene lifetimes (a few hours) are sufficiently short that a strong correlation with organic aerosol mass may not be expected. The particle composition is perturbed during the biogenic period by: (1) a plume from smelting operations in Sudbury, Ontario (~300 km to the north), leading to increased sulfate (overnight 11–12 June); and (2) a biomass burning event during the first half of 10 June.

ACPD
9, 18113–18158, 2009

The anthropogenic case study is characterized by southerly winds. Back trajectories indicate air masses passing over the Toronto urban area and populated regions to the south/southwest. Aromatic VOCs, NO_x, and particulate sulfate are all elevated. The high sulfate periods on 15 May, 24–25 May, and 9 June are examples of similar events, though of shorter duration.

The biomass burning period is characterized by high potassium and slightly elevated acetonitrile. BBOA concentrations are near their maximum for the study period. While potassium, acetonitrile, and BBOA are elevated and correlated at other periods during the study, this occurs during periods strongly influenced by anthropogenic emissions, making them unsuitable for examination of biomass burning aerosol.

As shown in Fig. 4, the organic composition during the biogenic event is characterized by increased OOA-2 relative to OOA-1 and very low BBOA and HOA. During the biogenic event, OOA-2 constitutes 65%±10% of the total OOA (i.e. OOA-1+OOA-2), vs. 46%±5% during periods of urban outflow (e.g. 30 May to 3 June). As discussed in the previous section, the correlation of OOA-2 with MACR+MVK during the biogenic period (R^2=0.71) indicates that the organic aerosol during the biogenic period is relatively fresh and therefore not the result of highly processed anthropogenic or biomass burning emissions. In contrast, OOA-1 is more strongly correlated with longer-lived photochemical oxidation products such as acetone, while HOA and BBOA correlate with tracers of primary emissions.

The biogenic period is distinguished by the relationship between the total organic material (OM) and OOA components with the CO mixing ratio, which are plotted against each other in Fig. 5 for the biogenic, biomass burning, and urban outflow periods identified in Fig. 4. CO is a long-lived species (lifetime on the order of a few months) that enters the atmosphere by direct emission from primary combustion and by gas-phase photochemistry, such as photolysis or OH-oxidation of formaldehyde. Figure 5a shows a dramatic difference in ΔOM/ΔCO between the biogenic period (234.4 $\mu g\,m^{-3}\,ppmv^{-1}$) vs. the urban outflow and biomass burning periods (71.1 $\mu g\,m^{-3}\,ppmv^{-1}$ and 109.1 $\mu g\,m^{-3}\,ppmv^{-1}$, respectively). Previous

ACPD
9, 18113–18158, 2009

measurements of ΔOM/ΔCO in anthropogenically-influenced regions (shaded region of Fig. 5a) have yielded values in the range of 10 to 85 $\mu g\,m^{-3}\,ppmv^{-1}$, with higher values corresponding to increased photochemical age (de Gouw et al., 2008; DeCarlo et al., 2008; Kleinman et al., 2009). Previous measurements of ΔOM/ΔCO in biomass burning plumes are also included. These values are estimated from $PM_{1.0}$/CO mass emission ratios in biomass burning plumes in Mexico City (0.133) and the Amazon (0.176) (Yokelson et al., 2007a, b), assuming that OM accounts for ~55% of the $PM_{1.0}$ mass (Reid et al., 2005). This provides a range of values from 91 to 121 $\mu g\,m^{-3}\,ppmv^{-1}$. Both the anthropogenic and biomass burning measurements at Egbert are consistent with previously measured values. However, the biogenic ΔOM/ΔCO is clearly distinct from either.

Figure 5c and d demonstrate that the difference in ΔOM/ΔCO between the biogenic and anthropogenic periods is driven by OOA-2. While ΔOOA-I/ΔCO is similar for the urban outflow and biogenic periods (38.2 $\mu g\,m^{-3}\,ppmv^{-1}$ vs. 43.5 $\mu g\,m^{-3}\,ppmv^{-1}$), ΔOOA-2/ΔCO is highly source-dependent (anthropogenic: 17.0 $\mu g\,m^{-3}\,ppmv^{-1}$ vs. biogenic: 145.6 $\mu g\ m^{-3}\ ppmv^{-1}$). The biomass burning period is distinct from either period, with OM dominated by BBOA. The biomass burning ΔOOA-2/ΔCO (39.2 $\mu g\,m^{-3}\,ppmv^{-1}$) more closely resembles urban outflow, while biomass burning OOA-1 remains at low, near-constant levels independent of CO (ΔOOA-I/ΔCO=0.4 $\mu g\,m^{-3}\,ppmv^{-1}$). The tight correlation between OOA-2 and CO for the biomass burning and biogenic periods in Fig. 5d suggests a relatively constant photochemical age. These correlations, coupled with the lack of intermediate points between the ΔOOA-2/ΔCO lines for the biomass burning and biogenic periods as would arise with photochemical aging, indicate that the organic concentrations during the biogenic period cannot be explained by aged biomass burning emissions. Further discussion of potential biomass burning influences is presented in Sect. 3.3.3. The distinct ΔOOA-2/ΔCO relationships described above suggest that OOA-2 observed during the biogenic period can be identified as biogenic SOA. The OOA-1 source is more ambiguous, due to its increased age and similarity of ΔOOA-I/ΔCO between the biogenic

ACPD
9, 18113–18158, 2009

and anthropogenic periods. We therefore estimate the biogenic SOA concentration as bounded by that of OOA-2 and OOA-1+OOA-2, yielding a peak biogenic SOA concentration of 8 to 12 $\mu g\,m^{-3}$.

3.3 Model interpretation of the biogenic period

3.3.1 Photochemical CO production

The difference in ΔOOA/ΔCO slopes can be understood in terms of the differences in CO sources and production mechanisms. CO is likely dominated by primary emissions during the anthropogenic period; however such emissions are expected to be negligible during the biogenic period. Instead, the strong correlation of CO with OOA-II, which during this period is correlated with the photochemical products MACR+MVK, suggests a photochemical source. The mass yield of SOA from biogenic VOCs can be estimated from Fig. 5, as discussed below. We assume all CO above the global background during the biogenic period is photochemical. A chemical transport model for the study region predicts average enhancements due to biogenic processes of roughly 25 ppbv in mid-summer (Hudman et al., 2008), which is comparable to the observed CO increase of 60 ppbv determined from Fig. 5. We believe our results show the first direct observational evidence for a significant biogenic source of CO from coniferous forests.

The relationship of CO to biogenic VOC mixing ratios is calculated using a box model, with α-pinene selected as a surrogate for precursor VOCs. (As discussed later in Sect. 3.3.2, the AURAMS air quality model identifies monoterpenes as the dominant precursor VOCs). A subset of a near-explicit Master Chemical Mechanism (v3.1) (Saunders et al., 2003) describing α-pinene oxidation (928 reactions and 310 compounds) is chosen. In order to run the model, 48 inorganic reactions and 21 inorganic compounds have been combined with that subset for α-pinene. More details of relevant model settings can be found in the literature (Xia et al., 2008). For simplicity, the chemistry is run in a zero-dimensional box model at a fixed temperature of 25°C

ACPD
9, 18113–18158, 2009

without deposition. The photolysis rates in the box model are set to the latitude of the Egbert site (44.23° N).

The chemical system was studied for 246 combinations of initial α-pinene concentrations and NO_x emission rates. Specifically, 6 different initial α-pinene concentrations (1.0 ppbv to 10.0 ppbv) and 41 different NO_x emission rates (1.8×10^5 molecules s^{-1} to 1.8×10^7 molecules s^{-1} yielding mean NO_x concentrations of 0.05 to 20 ppbv) were chosen, with the concentrations and emission rates selected to be evenly spaced on a logarithmic scale. During the biogenic period, the measured NO_x concentrations were 1.02±0.74 ppbv, with a maximum of 4.72 ppbv (5 min average).

For each scenario, the model was run for 48 h from midnight, at which point the $\Delta CO/\Delta\alpha$-pinene ratio is calculated. It is found that the obtained ratios lie within 3.0±0.4. Results for the 48-h simulation are shown in Fig. 6. Beyond 48 h, the ratio continues to increase, reaching 3.4±0.4, 3.8±0.4, and 4.0±0.4 at 72 h, 120 h, and 360 h, respectively.

As discussed in the previous section, we estimate the lower and upper limits of the biogenic SOA to be OOA-2 and OOA-1+OOA-2, respectively. The slopes of Fig. 5b and c, for the biogenic period yield $\Delta SOA/\Delta CO$=146 to 189 $\mu g\,m^{-3}\,ppmv^{-1}$. From the MCM 48-h simulation ($\Delta CO/\Delta\alpha$-pinene=3.0±0.4), this equates to $\Delta SOA/\Delta\alpha$-pinene of 437 to 567 $\mu g\,m^{-3}\,ppmv^{-1}$, or a mass yield of 7.2 to 9.3%. These values are consistent with the literature, where reported SOA mass yields from α-pinene range from approximately 3 to 20%, although a direct comparison is complicated by the dependence of the yield on SOA mass loading (causing an increased yield), temperature, and high/low NO_x regimes (Griffin et al., 1999; Pathak et al., 2007; Shilling et al., 2008; Tunved et al., 2006).

3.3.2 Regional SOA production

AURAMS (A Unified Regional Air-Quality Monitoring System) (Moran et al., 1998) model output for four subsequent days during the biogenic event (10 to 13 June) are plotted in Figs. 7 and 8. Figure 7 shows spatial distributions of $PM_{2.5}$ SOA, while Fig. 8 shows surface temperature and wind fields for the same time periods. The figures indicate generation of organic aerosol over forested regions of Ontario and Quebec correlated with increased temperature, followed by transport southwest to the Egbert site. Back trajectories indicate that air is transported between these locations over approximately a day. The observed elevated mixing ratios of MACR+MVK and monoterpene oxidation products at Egbert are consistent with this timescale, because MACR and MVK have atmospheric lifetimes of approximately half a day (Biesenthal et al., 1998).

As shown in Fig. 9, the urban plume (7–9 June), smelter plume (sulfate, 12 June) and biogenic event (10–14 June) are well reproduced by AURAMS. The sensitivity of SOA concentrations to individual classes of VOC precursors was tested in AURAMS by removing SOA production from these precursors (Fig. 9, lower panel). Removal of SOA production by monoterpenes, sesquiterpenes, and isoprene decreased SOA mass concentrations by 65%, 4%, and 7%, respectively. This suggests that the high SOA concentrations during the biogenic event result primarily from oxidation of monoterpenes. This is consistent with one other report in the literature of high biogenic SOA mass, which was also observed in a region of high terpene emissions (Shantz et al., 2004).

The correlation between AMS measurements and AURAMS predictions of biogenic SOA in Fig. 9 suggest that the high loadings are due to high biogenic VOC emissions rather than unknown chemistry. Figure 8 shows temperatures in excess of 30°C across a wide geographical area. Because this region is dominated by monoterpene emissions, which increase exponentially with temperature (Guenther et al., 1991) and have a relatively high SOA yield, it is likely that the high temperatures are the driving force of the biogenic event.

ACPD
9, 18113–18158, 2009

3.3.3 Evaluation of potential biomass burning influences on the biogenic event

A crucial consideration for the biogenic SOA event discussed here is the extent to which influences from fresh or aged biomass burning aerosol can be ruled out. For clarity, we present elements of the above analysis specifically pertaining to biomass burning influences within this section. For this analysis, we distinguish between the influences of (1) fresh biomass burning and (2) aged biomass burning and discuss the two separately below.

For this discussion, "fresh" biomass burning is defined as the biomass burning contribution to OOA-2, which is identified as fresh by its correlation with MACR+MVK. The following observations suggest that the biomass burning influence is negligible during the biogenic case study:

1. Chemical markers of primary biomass burning emissions (potassium, acetonitrile, BBOA) are negligible (see Fig. 4). Indeed, the onset of the biogenic period is marked by a dramatic reduction in the concentrations of potassium and acetonitrile, contrary to what would occur if a biomass burning period were starting.

2. The ΔOM/ΔCO ratio for biogenics is significantly larger than observed in this study or reported in the literature (see Fig. 5a). Further, the difference is also pronounced in the ΔOOA-2/ΔCO ratio.

3. AURAMS accurately predicts SOA concentrations using biogenic (primarily monoterpene) emissions as precursors (see Fig. 9). No biomass burning contribution is required.

4. Analysis of MODIS fire counts (Fig. 10a) and HYSPLIT back trajectories (Fig. 10c) indicate negligible fire influence within half a day of the site. (It is estimated that the OOA-2 must be produced within half a day based on its correlations with MACR+MVK. This is also supported by AURAMS.)

ACPD
9, 18113–18158, 2009

Similar to the preceding discussion, "aged" biomass burning is here defined as the biomass burning contribution to OOA-1. While the source(s) of OOA-1 are more ambiguous than those of OOA-2, the following observations suggest that OOA-1 cannot be attributed to aged biomass burning emissions:

1. Chemical markers of primary biomass burning emissions (potassium, acetonitrile, BBOA) are negligible (see Fig. 4). Acetonitrile and potassium are relatively long-lived. The lifetime of BBOA is less certain.

2. Best agreement with AURAMS SOA predictions is obtained through comparison with OOA-1+OOA-2 (rather than OOA-2 alone), and AURAMS SOA precursors are dominated by monoterpenes (see Fig. 9).

3. Analysis of MODIS fire counts (Fig. 10a) and HYSPLIT 48-h back trajectories (Fig. 10c) are inconsistent with a long-range fire source. Although the trajectories during the final two days of the biogenic period pass near a fire-influenced area, the fires do not begin until after the airmass has passed through. Further, these fires are close enough that significant enhancements in chemical markers of biomass burning would be expected, which as discussed in point (1) does not occur. Finally, the fire counts to the northeast of the site in Fig. 10a represent the only major fires in Canada during the biogenic period.

4. As shown in Fig. 10c, the trajectories during the biogenic period originate from a variety of locations north of Egbert. Given that biomass burning emissions are expected to be localized (e.g. Fig. 10a), the observed tight correlation between organic mass and CO is not consistent with biomass burning origins, as the SOA/CO ratio will depend on photochemical age when the CO is dominated by primary emissions. However, a tight correlation between organics and CO is in fact observed (see Fig. 5) and is consistent with photochemically-generated CO from a widespread biogenic source from forested regions.

ACPD
9, 18113–18158, 2009

3.4 Regional impact of biogenic SOA

Remote sensing measurements suggest that the high levels of particulate organics observed in this study are representative of the regional contribution of biogenic VOC emissions. This is shown in Fig. 9 by the correlated increases of observed and modeled biogenic SOA with the regional AOD, measured by the MODIS satellite instrument (Salomonson et al., 1989) for the box defined by 44° to 47° N and 77° to 80° W, containing Egbert in its southwest corner. Figure 10a shows the AOD over northern Ontario and Quebec during the biogenic period (9 to 13 June), with the locations of Egbert and the previously described box displayed. A widespread region of elevated AOD exists over the sparsely populated, boreal forest region to the north of the sampling location. MODIS fire counts to the north are negligible, though some fires were observed in regions to the northeast. Back trajectories (48-h duration) from the Egbert site are shown in Fig. 10c. Contamination from the single fire count detected to the southwest is unlikely given its short duration (a single day), prevailing northerly winds, and measured aerosol composition.

Figure 10b shows the monthly averages of AOD from 2001 to 2006 for the boxed region, suggesting that this biogenic radiative forcing effect is strongest in the late spring and early summer. A similar seasonal cycle has been observed in the southeast United States (Goldstein et al., 2009), where isoprene is the dominant biogenic VOC. Egbert mean AOD during summer is typically lower than that reported by Goldstein et al. (~0.16 vs. ~0.35). The lower values at Egbert are probably due to (1) lower temperatures and (2) decreased anthropogenic influence. However, Egbert AOD climbed to 0.23 during the biogenic event, with significantly higher values (~0.4) farther north (see Fig. 10a).

The increased AOD will have a significant regional cooling effect in clear-sky conditions over a (relatively dark) forest. Globally averaged, the estimated direct aerosol radiative forcing is at least that of the CO_2 generated from the photochemically-produced biogenic CO over the entire CO_2 lifetime. As an example, radiative forcing estimates

ACPD
9, 18113–18158, 2009

for the CO_2 from biogenic CO and for the biogenic aerosol were made using the radiation algorithm described by Li and Barker (Li and Barker, 2005) as applied in the Canadian GCM, for clear sky conditions. For an aerosol optical depth of 0.2, the net upward flux at 200 mb was calculated to increase by 20 W m^{-2} (−661.2 W m^{-2} to −681.2 W m^{-2}). Using the standard North American atmospheric profile, the CO_2 increase of 0.06 ppm was calculated to decrease the net upward flux by 0.0011 W m^{-2} at 200 mb (230.5757 W m^{-2} for 370 ppm and 230.5746 W m^{-2} for 370.06 ppm). Assuming a one week lifetime for the aerosol and a 100 year lifetime for the CO_2, we calculate the relative forcing potential of the two as −20*7/(0.0011*365*100), yielding a relative cooling factor of −3.5. This value will be reduced when cloud cover is considered and is subject to assumptions of surface albedo, aerosol absorption, etc.

Further cooling will result from the cloud condensation nuclei activity of the biogenic SOA, which reached a maximum value of ∼1600 cm^{-3} during the biogenic period (0.42% supersaturation) vs. ∼3000 cm^{-3} during the 30 May to 3 June urban outflow period. The high particle concentration and CCN activity are consistent with a significant contribution to climate forcing from biogenic aerosol arising from mid-latitude forests, as suggested by a recent modeling study (Spracklen et al., 2008).

4 Conclusions

Organic concentrations reaching levels ∼5 times higher than most previous measurements for biogenic aerosols are observed, likely resulting from elevated temperatures and VOC emissions from Canadian coniferous forests. Biogenic OM is identified from correlations with tracer VOCs and by the relationship of the total OM and oxygenated components with CO. The observations provide evidence for a significant photochemical source of biogenic CO. Biogenic SOA concentrations are accurately predicted by a regional air quality model, in contrast to model underpredictions reported in more polluted regions. Model calculations and remote sensing measurements indicate that the high mass loading is widespread, implying that biogenic SOA contributes strongly

ACPD
9, 18113–18158, 2009

to the regional aerosol, presumably in both rural and urban locations in Southern Ontario. The high particle concentration and CCN activity are consistent with a significant contribution to climate forcing from biogenic aerosol arising from mid-latitude forests.

Acknowledgements. This work was supported by the Canadian Foundation for Climate and Atmospheric Sciences through the Cloud-Aerosol Feedbacks and Climate Network and by the Natural Science and Engineering Research Council (Canada). Partial infrastructure funding came from CFI and OIT. The authors also thank J. Li for discussion of the radiative forcing calculations, R. Volkamer for discussion of the SOA yield calculation, and the MODIS team for measurements of aerosol optical depth.

References

Aiken, A. C., DeCarlo, P. F., Kroll, J. H., Worsnop, D. R., Huffman, J. A., Docherty, K. S., Ulbrich, I. M., Mohr, C., Kimmel, J. R., Sueper, D., Sun, Y., Zhang, Q., Trimborn, A., Northway, M., Ziemann, P. J., Canagaratna, M. R., Onasch, T. B., Alfarra, M. R., Prevot, A. S. H., Dommen, J., Duplissy, J., Metzger, A., Baltensperger, U., and Jimenez, J. L.: O/C and OM/OC Ratios of Primary, Secondary, and Ambient Organic Aerosols with High-Resolution Time-of-Flight Aerosol Mass Spectrometry, Environ. Sci. Technol., 42, 4478–4485, doi:10.1021/es703009q, 2008.

Aiken, A. C., Salcedo, D., Cubison, M. J., Huffman, J. A., DeCarlo, P. F., Ulbrich, I. M., Docherty, K. S., Sueper, D., Kimmel, J. R., Worsnop, D. R., Trimborn, A., Northway, M., Stone, E. A., Schauer, J. J., Volkamer, R., Fortner, E., de Foy, B., Wang, J., Laskin, A., Shutthanandan, V., Zheng, J., Zhang, R., Gaffney, J., Marley, N. A., Paredes-Miranda, G., Arnott, W. P., Molina, L. T., Sosa, G., and Jimenez, J. L.: Mexico City aerosol analysis during MILAGRO using high resolution aerosol mass spectrometry at the urban supersite (T0) - Part 1: Fine particle composition and organic source apportionment, Atmos. Chem. Phys. Discuss., 9, 8377–8427, 2009, http://www.atmos-chem-phys-discuss.net/9/8377/2009/.

Allan, J. D., Jimenez, J. L., Williams, P. I., Alfarra, M. R., Bower, K. N., Jayne, J. T., Coe, H., and Worsnop, D. R.: Quantitative sampling using an Aerodyne aerosol mass spectrometer 1: Techniques of data interpretation and error analysis, J. Geophys. Res., 108, 4090, doi:10.1029/2002JD002358, 2003.

Biesenthal, T. A., Bottenheim, J. W., Shepson, P. B., Li, S.-M., and Brickell, P. C.: The chemistry of biogenic hydrocarbons at a rural site in eastern Canada, J. Geophys. Res., 103, 25487–25498, 1998.

Brickell, P. C., Bottenheim, J. W., Froude, F., and Jiang, Z.: In-Situ NMHC Measurements in Rural Ontario, Canada, Eos. Trans. AGU, Fall Meeting, A31D-0070, 2003.

Canagaratna, M. R., Jayne, J. T., Jimenez, J. L., Allan, J. D., Alfarra, M. R., Zhang, Q., Onasch, T. B., Drewnick, F., Coe, H., Middlebrook, A. M., Delia, A., Williams, L. R., Trimborn, A. M., Northway, M. J., DeCarlo, P. F., Kolb, C. E., Davidovits, P., and Worsnop, D. R.: Chemical and microphysical characterization of ambient aerosols with the Aerodyne aerosol mass spectrometer, Mass Spectrom. Rev., 26, 185–222, 2007.

Capes, G., Murphy, J. G., Reeves, C. E., McQuaid, J. B., Hamilton, J. F., Hopkins, J. R., Crosier, J., Williams, P. I., and Coe, H.: Secondary organic aerosol from biogenic VOCs over West Africa during AMMA, Atmos. Chem. Phys., 9, 3841–3850, 2009, http://www.atmos-chem-phys.net/9/3841/2009/.

CEP, Carolina Environmental Program, Sparse Matrix Operator Kernel Emission (SMOKE) modelling system, pp. see http://www.smoke-model.org/index.cfm, last access: 2009, University of North Carolina, Carolina Environmental Programs, Chapel Hill, NC, 2003.

Chang, R.Y.-W., Liu, P. S. K., Leaitch, W. R., and Abbatt, J. P. D.: Comparison between measured and predicted CCN concentrations at Egbert, Ontario: Focus on the organic aerosol fraction at a semi-rural site, Atmos. Environ., 41, 8172–8182, 2007.

Claeys, M., Braham, B., Vas, G., Wang, W., Vermeylen, R., Pashynska, V., Cafmeyer, J., Guyon, P., Andreae, M. O., Artaxo, P., and Maenhaut, W.: Formation of Secondary Organic Aerosols Through Photooxidation of Isoprene, Science, 303, 1173–1176, 2004.

Côté, J., Desmarais, J.-G., Gravel, S., Méthot, A., Patoine, A., Roch, M., and Staniforth, A.: The operational CMC-MRB global environmental multiscale (GEM) model, Part I: Design considerations and formulation, Mon. Weather Rev., 126, 1373–1395, 1998a.

Côté, J., Desmarais, J.-G., Gravel, S., Méthot, A., Patoine, A., Roch, M., and Staniforth, A.: The operational CMC-MRB global environmental multiscale (GEM) model, Part II: Results, Mon. Weather Rev., 126, 1373–1395, 1998b.

Cross, E. S., Onasch, T. B., Canagaratna, M., Jayne, J. T., Kimmel, J., Yu, X.-Y., Alexander, M. L., Worsnop, D. R., and Davidovits, P.: Single particle characterization using a light scattering module coupled to a time-of-flight aerosol mass spectrometer, Atmos. Chem. Phys. Discuss., 8, 21313–21381, 2008,

http://www.atmos-chem-phys-discuss.net/8/21313/2008/.
Cross, E. S., Slowik, J. G., Davidovits, P., Allan, J. D., Worsnop, D. R., Jayne, J. T., Lewis, D. K., Canagaratna, M. R., and Onasch, T. B.: Laboratory and Ambient Particle Density Determinations using Light Scattering in Conjunction with Aerosol Mass Spectrometry, Aerosol Sci. Tech., 41, 343–359, doi:10.1080/02786820701199736, 2007.
de Gouw, J. A., Brock, C. A., Atlas, E. L., Bates, T. S., Fehsenfeld, F. C., Goldan, P. D., Holloway, J. S., Kuster, W. C., Lerner, B. M., Matthew, B. M., Middlebrook, A. M., Onasch, T. B., Peltier, R. E., Quinn, P. K., Senff, C. J., Stohl, A., Sullivan, A. P., Trainer, M., Warneke, C., Weber, R. L., and Williams, E. J.: Sources of particulate matter in the northeastern United States in summer: 1, Direct emissions and secondary formation of organic matter in urban plumes, J. Geophys. Res., 113, D08301, doi:10.1029/2007JD009243, 2008.
de Gouw, J. A. and Warneke, C.: Measurements of volatile organic compounds in the Earth's atmosphere using proton-transfer-reaction mass spectrometry, Mass Spectrom. Rev., 26, 223–257, 2007.
DeCarlo, P. F., Dunlea, E. J., Kimmel, J. R., Aiken, A. C., Sueper, D., Crounse, J., Wennberg, P. O., Emmons, L., Shinozuka, Y., Clarke, A., Zhou, J., Tomlinson, J., Collins, D. R., Knapp, D., Weinheimer, A. J., Montzka, D. D., Campos, T., and Jimenez, J. L.: Fast airborne aerosol size and chemistry measurements above Mexico City and Central Mexico during the MILAGRO campaign, Atmos. Chem. Phys., 8, 4027–4048, 2008, http://www.atmos-chem-phys.net/8/4027/2008/.
DeCarlo, P. F., Kimmel, J. R., Trimborn, A., Northway, M. J., Jayne, J. T., Aiken, A. C., Gonin, M., Fuhrer, K., Horvath, T., Docherty, K. S., Worsnop, D. R., and Jimenez, J. L.: Field-Deployable, High-Resolution, Time-of-Flight Aerosol Mass Spectrometer, Anal. Chem., 78, 8281–8289, 2006.
Drewnick, F., Hings, S. S., Curtius, J., Eerdekens, G., and Williams, J.: Measurement of fine particulate and gas-phase species during the New Year's fireworks 2005 in Mainz, Germany, Atmos. Environ., 40, 4316–4327, 2006.
Drewnick, F., Hings, S. S., DeCarlo, P. F., Jayne, J. T., Gonin, M., Fuhrer, K., Weimer, S., Jimenez, J. L., Demerjian, K. L., Borrmann, S., and Worsnop, D. R.: A new Time-of-Flight Aerosol Mass Spectrometer (ToF-AMS) – Instrument description and first field deployment, Aerosol Sci. Tech.., 39, 637–658, 2005.
Dzepina, K., Volkamer, R. M., Madronich, S., Tulet, P., Ulbrich, I. M., Zhang, Q., Cappa, C. D., Ziemann, P. J., and Jimenez, J. L.: Evaluation of recently-proposed secondary organic

aerosol models for a case study in Mexico City, Atmos. Chem. Phys., 9, 5681–5709, 2009, http://www.atmos-chem-phys.net/9/5681/2009/.
Giglio, L., Descloitres, J., Justice, C. O., and Kaufman, Y. J.: An Enhanced Contextual Fire Detection Algorithm for MODIS, Remote Sens. Environ., 87, 273–282, 2003.
Goldstein, A. H. and Galbally, I. E.: Known and Unexplored Organic Constituents in the Earth's Atmosphere, Environ. Sci. Technol., 41, 1514–1521, 2007.
Goldstein, A. H., Koven, C. D., Heald, C. L., and Fung, I. Y.: Biogenic carbon and anthropogenic pollutants combine to form a cooling haze over the southeastern United States, P. Natl. Acad. Sci., 106, 8835–8840, doi:10.1073/pnas.0904128106, 2009.
Gong, S. L., Barrie, L. A., Blanchet, J.-P., von Salzen, K., Lohmann, U., Lesins, G., Spacek, L., Zhang, L. M., Girard, E., Lin, H., Leaitch, W. R., Leighton, H., Chylek, P., and Huang, P.: Canadian Aerosol Module: A size-segregated simulation of atmospheric aerosol processes for climate and air quality models, 1, Module development, J. Geophys. Res.-Atmos., 108, AAC 3-1–AAC 3-16, 2003.
Griffin, R. J., Cocker III, D. R., Flagan, R. C., and Seinfeld, J. H.: Organic aerosol formation from the oxidation of biogenic hydrocarbons, J. Geophys. Res.-Atmos., 104, 3555–3567, 1999.
Guenther, A., Geron, C., Pierce, T., Lamb, B., Harley, P., and Fall, R.: Natural emissions of non-methane volatile organic compounds, carbon monoxide, and oxides of nitrogen from North America, Atmos. Environ., 34, 2205–2230, 2000.
Guenther, A., Otter, L., Zimmerman, P., Greenberg, J., Scholes, R., and Scholes, M.: Biogenic hydrocarbon emissions from southern African savannas, J. Geophys. Res., 101, 25859–25865, 1996.
Guenther, A. B., Monson, R. K., and Fall, R.: Isoprene and Monoterpene Emission Rate Variability: Observations With Eucalyptus and Emission Rate Algorithm Development, J. Geophys. Res., 96, 10799–10808, 1991.
Gunthe, S. S., King, S. M., Rose, D., Chen, Q., Roldin, P., Farmer, D. K., Jimenez, J. L., Artaxo, P., Andreae, M. O., Martin, S. T., and Pöschl, U.: Cloud condensation nuclei in pristine tropical rainforest air of Amazonia: size-resolved measurements and modeling of atmospheric aerosol composition and CCN activity, Atmos. Chem. Phys. Discuss., 9, 3811–3870, 2009, http://www.atmos-chem-phys-discuss.net/9/3811/2009/.
Hallquist, M., Wenger, J. C., Baltensperger, U., Rudich, Y., Simpson, D., Claeys, M., Dommen, J., Donahue, N. M., George, C., Goldstein, A. H., Hamilton, J. F., Herrmann, H., Hoffmann,

T., Iinuma, Y., Jang, M., Jenkin, M. E., Jimenez, J. L., Kiendler-Scharr, A., Maenhaut, W., McFiggans, G., Mentel, Th. F., Monod, A., Prévôt, A. S. H., Seinfeld, J. H., Surratt, J. D., Szmigielski, R., and Wildt, J.: The formation, properties and impact of secondary organic aerosol: current and emerging issues, Atmos. Chem. Phys., 9, 5155–5235, 2009, http://www.atmos-chem-phys.net/9/5155/2009/.

Helmig, D., Ortega, J., Duhl, T., Tanner, D., Guenther, A., Harley, P., Wiedinmyer, C., Milford, J., and Sakulyanontvittaya, T.: Sesquiterpene emissions from pine trees – identifications, emission rates and flux estimates for the contiguous United States, Environ. Sci. Technol., 41, 1545–1553, 2007.

Henze, D. K., Seinfeld, J. H., Ng, N. L., Kroll, J. H., Fu, T.-M., Jacob, D. J., and Heald, C. L.: Global modeling of secondary organic aerosol formation from aromatic hydrocarbons: high- vs. low-yield pathways, Atmos. Chem. Phys., 8, 2405–2420, 2008, http://www.atmos-chem-phys.net/8/2405/2008/.

Hildebrandt, L., Donahue, N. M., and Pandis, S. N.: High formation of secondary organic aerosol from the photo-oxidation of toluene, Atmos. Chem. Phys., 9, 2973–2986, 2009, http://www.atmos-chem-phys.net/9/2973/2009/.

Houyoux, M. R., Vukovich, J. M., Coats, C. J. J., and Wheeler, N. J. M.: Emission inventory development and processing for the Season Model for Regional Air Quality (SMRAQ) project, J. Geophys. Res., 105, 9079–9090, 2000.

Hudman, R. C., Murray, L. T., Jacob, D. J., Millet, D. B., Turquety, S., Wu, S., Blake, D. R., Goldstein, A. H., Holloway, J., and Sachse, G. W.: Biogenic versus anthropogenic sources of CO in the United States, Geophys. Res. Lett., 35, L04801, doi:10.1029/2007GL032393, 2008.

Huffman, J. A., Docherty, K. S., Aiken, A. C., Cubison, M. J., Ulbrich, I. M., DeCarlo, P. F., Sueper, D., Jayne, J. T., Worsnop, D. R., Ziemann, P. J., and Jimenez, J. L.: Chemically-resolved aerosol volatility measurements from two megacity field studies, Atmos. Chem. Phys. Discuss., 9, 2645–2697, 2009, http://www.atmos-chem-phys-discuss.net/9/2645/2009/.

Jayne, J. T., Leard, D. C., Zhang, X. F., Davidovits, P., Smith, K. A., Kolb, C. E., and Worsnop, D. R.: Development of an Aerosol Mass Spectrometer for Size and Composition Analysis of Submicron Particles, Aerosol Sci. Tech., 33, 49–70, 2000.

Jimenez, J. L., Jayne, J. T., Shi, Q., Kolb, C. E., Worsnop, D. R., Yourshaw, I., Seinfeld, J. H., Flagan, R. C., Zhang, X. F., Smith, K. A., Morris, J. W., and Davidovits, P.: Ambi-

ent Aerosol Sampling with an Aerosol Mass Spectrometer, J. Geophys. Res., 108, 8425, doi:8410:1029/2001JD001213, 2003.
Johnson, D., Utembe, S. R., Jenkin, M. E., Derwent, R. G., Hayman, G. D., Alfarra, M. R., Coe, H., and McFiggans, G.: Simulating regional scale secondary organic aerosol formation during the TORCH 2003 campaign in the southern UK, Atmos. Chem. Phys., 6, 403–418, 2006, http://www.atmos-chem-phys.net/6/403/2006/.
Kanakidou, M., Seinfeld, J. H., Pandis, S. N., Barnes, I., Dentener, F. J., Facchini, M. C., Van Dingenen, R., Ervens, B., Nenes, A., Nielsen, C. J., Swietlicki, E., Putaud, J. P., Balkanski, Y., Fuzzi, S., Horth, J., Moortgat, G. K., Winterhalter, R., Myhre, C. E. L., Tsigaridis, K., Vignati, E., Stephanou, E. G., and Wilson, J.: Organic aerosol and global climate modelling: a review, Atmos. Chem. Phys., 5, 1053–1123, 2005, http://www.atmos-chem-phys.net/5/1053/2005/.
Kavouras, I. G., Mihalopoulos, M., and Stephanou, E. G.: Formation of atmospheric particles from organic acids produced by forests, Nature, 395, 683–686, 1998.
Kleinman, L. I., Springston, S. R., Wang, J., Daum, P. H., Lee, Y.-N., Nunnermacker, L. J., Senum, G. I., Weinstein-Lloyd, J., Alexander, M. L., Hubbe, J., Ortega, J., Zaveri, R. A., Canagaratna, M. R., and Jayne, J.: The time evolution of aerosol size distribution over the Mexico City plateau, Atmos. Chem. Phys., 9, 4261–4278, 2009, http://www.atmos-chem-phys.net/9/4261/2009/.
Kroll, J. H., Ng, N. L., Murphy, S. M., Flagan, R. C., and Seinfeld, J. H.: Secondary aerosol formation from isoprene photooxidaation, Environ. Sci. Technol., 40, 1869–1877, 2006.
Kuhn, M., Builtjes, P. J. H., Poppe, D., Simpson, D., Stockwell, W. R., Andersson-Sköld, Y., Baart, A., Das, M., Fiedler, F., Hov, Ø., Kirchner, F., Makar, P. A., Milford, J. B., Roemer, M. G. M., Ruhnke, R., Strand, A., Vogel, B., and Vogel, H.: Intercomparison of the gas-phase chemistry in several chemistry and transport models, Atmos. Environ., 32, 693–709, 1998.
Kumar, P. P., Broekhuizen, K., and Abbatt, J. P. D.: Organic acids as cloud condensation nuclei: Laboratory studies of highly soluble and insoluble species, Atmos. Chem. Phys., 3, 509–520, 2003, http://www.atmos-chem-phys.net/3/509/2003/.
Lane, T. E., Donahue, N. M., and Pandis, S. N.: Effect of NO_x on secondary organic aerosol concentrations, Environ. Sci. Technol., 42, 6022–6027, 2008.
Lanz, V. A., Alfarra, M. R., Baltensperger, U., Buchmann, B., Hueglin, C., and Prévôt, A. S.

H.: Source apportionment of submicron organic aerosols at an urban site by factor analytical modelling of aerosol mass spectra, Atmos. Chem. Phys., 7, 1503–1522, 2007, http://www.atmos-chem-phys.net/7/1503/2007/.

Lanz, V. A., Alfarra, M. R., Baltensperger, U., Buchmann, B., Hueglin, C., Szidat, S., Wehrli, M. N., Wacker, L., Weimer, S., Caseiro, A., Puxbaum, H., and Prevot, A. S. H.: Source Attribution of Submicron Organic Aerosols during Wintertime Inversions by Advanced Factor Analysis of Aerosol Mass Spectra, Environ. Sci. Technol., 42, 214–220, 2008.

Lee, A., Goldstein, A. H., Keywood, M. D., Gao, S., Varutbangkul, V., Bahreini, R., Ng, N. L., Flagan, R. C., and Seinfeld, J. H.: Gas-phase products and secondary aerosol yields from the ozonolysis of ten different terpenes, J. Geophys. Res., 111, D07302, doi:10.1029/2005JD006437, 2006a.

Lee, A., Goldstein, A. H., Kroll, J. H., Ng, N. L., Varutbangkul, V., Flagan, R. C., and Seinfeld, J. H.: Gas-phase products and secondary aerosol yields from the photooxidation of 16 different terpenes, J. Geophys. Res., 111, D17305, doi:10.1029/2006JD007050, 2006b.

Levy, R. C., Remer, L. A., Mattoo, S., Vermote, E. F., and Kaufman, Y. J.: Second-generation operational algorithm: Retrieval of aerosol properties over land from inversion of Moderate Resolution Imaging Spectroradiometer Spectral reflectance, J. Geophys. Res., 112, D13211, doi:10.1029/2006JD007811, 2007.

Li, J. and Barker, H. W.: A radiation algorithm with correlated k-distribution, Part I: local thermal equilibrium, J. Atmos. Sci., 62, 286–309, 2005.

Lindinger, W., Hansel, A., and Jordan, A.: Proton-transfer reaction mass spectrometry (PTR-MS): on-line monitoring of volatile organic compounds at pptv levels, Chem. Soc. Rev., 27, 347–354, 1998.

Matthew, B. M., Middlebrook, A. M., and Onasch, T. B.: Collection Efficiencies in an Aerodyne Aerosol Mass Spectrometer as a Function of Particle Phase for Laboratory Generated Aerosols, Aerosol Sci. Tech., 42, 884–898, 2008.

Moran, M. D., Dastoor, A., Gong, S. L., Gong, W., and Makar, P. A.: Proposed Conceptual Design for the AES Regional Particulate Matter Model/Unified Model, pp. 100 (Available from first author), Meteorological Service of Canada, Downsview, ON, Canada, 1998.

Ng, N. L., Kroll, J. H., Chan, A. W. H., Chhabra, P. S., Flagan, R. C., and Seinfeld, J. H.: Secondary organic aerosol formation from m-xylene, toluene, and benzene, Atmos. Chem. Phys., 7, 3909–3922, 2007, http://www.atmos-chem-phys.net/7/3909/2007/.

Odum, J. R., Hoffman, T., Bowman, F., Collins, D., Flagan, R. C., and Seinfeld, J. H.: Gas/particle partitioning and secondary organic aerosol yields, Environ. Sci. Technol., 8, 2580–2585, 1996.

Paatero, P.: Least squares formulation of robust non-negative factor analysis, Chemometr. Intell. Lab., 37, 23-35, 1997.

Paatero, P. and Tapper, U.: Positive Matrix Factorization: A non-negative factor model with optimal utilization of error estimates of data values, Environmetrics, 5, 111–126, 1994.

Pathak, R. K., Presto, A. A., Lane, T. E., Stanier, C. O., Donahue, N. M., and Pandis, S. N.: Ozonolysis of α-pinene: parameterization of secondary organic aerosol mass fraction, Atmos. Chem. Phys., 7, 3811–3821, 2007, http://www.atmos-chem-phys.net/7/3811/2007/.

Presto, A. A. and Donahue, N. M.: Investigation of α-pinene+ozone secondary organic aerosol formation at low total aerosol mass, Environ. Sci. Technol., 40, 3536–3543, 2006.

Rappenglück, B., Apel, E., Bauerfeind, M., Bottenheim, J. W., Brickell, P. C., Cavolka, P., Cech, J., Gatti, L., Hakola, H., Honzak, J., Junek, R., Martin, D., Noone, C., Plass-Dülmer, C., Travers, D., and Wang, D.: The first VOC intercomparison exercise within the Global Atmosphere Watch (GAW), Atmos. Environ., 40, 7508–7527, 2006.

Reid, J. S., Koppmann, R., Eck, T. F., and Eleuterio, D. P.: A review of biomass burning emissions part II: intensive physical properties of biomass burning particles, Atmos. Chem. Phys., 5, 799–825, 2005, http://www.atmos-chem-phys.net/5/799/2005/.

Remer, L. A., Kaufman, Y. J., Tanre, D., Mattoo, S., Chu, D. A., Martins, J. V., Li, R.-R., Ichoku, C., Levy, R. C., Kleidman, R. G., Eck, T. F., Vermote, E. F., and Holben, B. N.: The MODIS Aerosol Algorithm, Products and Validation, J. Atmos. Sci., Special Section, 62, 947–973, 2005.

Rupakheti, M., Leaitch, W. R., Lohmann, U., Hayden, K. L., Brickell, P., Lu, G., Li, S.-M., Toom-Sauntry, D., Bottenheim, J. W., Brook, J. R., Vet, R., Jayne, J. T., and Worsnop, D. R.: An Intensive Study of the Size and Composition of Submicron Atmospheric Aerosols at a Rural Site in Ontario, Canada, Aerosol Sci. Tech., 39, 722–736, 2005.

Salomonson, V. V., Barnes, W. L., Maymon, P. W., Montgomery, H. E., and Ostrow, H.: MODIS: Advanced Facility Instrument for Studies of the Earth as a System, IEEE T. Geosci. Remote, 27, 145–153, 1989.

Sandu, A. and Sander, R.: Technical note: Simulating chemical systems in Fortran90 and

ACPD

9, 18113–18158, 2009

Matlab with the Kinetic PreProcessor KPP-2.1, Atmos. Chem. Phys., 6, 187–195, 2006, http://www.atmos-chem-phys.net/6/187/2006/.

Saunders, S. M., Jenkin, M. E., Derwent, R. G., and Pilling, M. J.: Protocol for the development of the Master Chemical Mechanism, MCM v3 (Part A): tropospheric degradation of non-aromatic volatile organic compounds, Atmos. Chem. Phys., 3, 161–180, 2003, http://www.atmos-chem-phys.net/3/161/2003/.

Schneider, J., Weimer, S., Drewnick, F., Borrmann, S., Helas, G., Gwaze, P., Schmid, O., Andreae, M. O., and Kirchner, U.: Mass spectrometric analysis and aerodynamic properties of various types of combustion-related aerosol particles, Int. J. Mass Spectrom., 258, 37–49, 2006.

Shantz, N. C., Aklilu, Y.-A., Ivanis, N., Leaitch, W. R., Brickell, P. C., Brook, J. R., Cheng, Y., Halpin, D., Li, S.-M., Tham, Y. A., Toom-Sauntry, D., Prenni, A. J., and Graham, L.: Chemical and physical observations of particulate matter at Golden Ears Provinical Park from anthropogenic and biogenic sources, Atmos. Environ., 38, 5849–5860, 2004.

Shilling, J. E., Chen, Q., King, S. M., Rosenoern, T., Kroll, J. H., Worsnop, D. R., McKinney, K. A., and Martin, S. T.: Particle mass yield in secondary organic aerosol formed by the dark ozonolysis of α-pinene, Atmos. Chem. Phys., 8, 2073–2088, 2008, http://www.atmos-chem-phys.net/8/2073/2008/.

Slowik, J. G., Vlasenko, A., McGuire, M., Evans, G. J., and Abbatt, J. P. D.: Simultaneous factor analysis of organic particle and gas mass spectra: AMS and PTR-MS measurements at an urban site, Atmos. Chem. Phys. Discuss., 9, 6739–6785, 2009, http://www.atmos-chem-phys-discuss.net/9/6739/2009/.

Smyth, S. C., Jiang, W., Roth, H., Moran, M. D., Makar, P. A., Yang, F., Bouchet, V. S., and Landry, H.: A comparative performance evaluation of the AURAMS and CMAQ air-quality modelling systems, Atmos. Environ., 43, 1059–1070, 2009.

Spracklen, D. V., Bonn, B., and Carslaw, K. S.: Boreal Forests, Aerosols and the Impacts on Clouds and Climate, Philos. T. R. Soc. A., 366, 4613–4626, 2008.

Stroud, C. A., Morneau, G., Makar, P. A., Moran, M. D., Gong, W., Pabla, B., Bouchet, V. S., Fox, D., Venkatesh, S., Wang, D., and Dann, T.: OH-reactivity of volatile organic compounds at urban and rural sites across Canada: Evaluation of air quality model predictions using speciated VOC measurements, Atmos. Environ., 42, 7746–7756, 2008.

Szidat, S., Jenk, T. M., Gäggeler, H. W., Synal, H.-A., Fisseha, R., Baltensperger, U., Kalberer, M., Samburova, V., Reimann, S., Kasper-Giebl, A., and Hajdas, I.: Radiocarbon (^{14}C)-

deduced biogenic and anthropogenic contributions to organic carbon (OC) of urban aerosols from Zürich, Switzerland, Atmos. Environ., 38, 4035–4044, 2004.
Tunved, P., Hansson, H.-C., Kerminen, V.-M., Ström, J., Dal Maso, M., Lihavainen, H., Viisanen, Y., Aalto, P. P., Komppula, M., and Kulmala, M.: High Natural Aerosol Loading over Boreal Forests, Science, 312, 261–263, 2006.
Ulbrich, I. M., Canagaratna, M. R., Zhang, Q., Worsnop, D. R., and Jimenez, J. L.: Interpretation of organic components from Positive Matrix Factorization of aerosol mass spectrometric data, Atmos. Chem. Phys., 9, 2891–2918, 2009, http://www.atmos-chem-phys.net/9/2891/2009/.
Ulbrich, I. M., Lechner, M., and Jimenez, J. L.: AMS Spectral Database, http://cires.colorado.edu/jimenez-group/AMSsd/, last access: 2009, 2009b.
Vlasenko, A., Slowik, J. G., Bottenheim, J. W., Brickell, P. C., Chang, R. Y.-W., Leaitch, W. R., Macdonald, A. M., Shantz, N. C., Sjostedt, S. J., Tham, A., Wiebe, H. A., and Abbatt, J. P. D.: VOC measurements at a rural Ontario site: Characterization of sources and connections to aerosol composition, J. Geophys. Res., submitted, 2009.
Volkamer, R., Jimenez, J. L., San Martini, F., Dzepina, K., Zhang, Q., Salcedo, D., Molina, L. T., Worsnop, D. R., and Molina, M. J.: Secondary organic aerosol formation from anthropogenic air pollution: Rapid and higher than expected, Geophys. Res. Lett., 33, L17811, doi:1029/2006GL026899, 2006.
Weber, R. J., Sullivan, A. P., Peltier, R. E., Russell, A., Yan, B., Zheng, M., De Gouw, J. A., Warneke, C., Brock, C. A., Holloway, J. S., Atlas, E. L., and Edgerton, E.: A study of secondary organic aerosol formation in the anthropogenic-influenced southeastern United States, J. Geophys. Res., 112, D13302, doi:10.1029/2007JD008408, 2007.
Williams, B. J., Goldstein, A. H., Millett, D. B., Holzinger, R., Kreisberg, N. M., Hering, S. V., White, A. B., Worsnop, D. R., Allan, J. D., and Jimenez, J. L.: Chemical speciation of organic aerosol during the Internation Consortium for Atmospheric Research on Transport and Transformation 2004: Results from in situ measurements, J. Geophys. Res., 112, D10S26, doi:10.1029/2006JD007601, 2007.
Xia, A. G., Michelangeli, D. V., and Makar, P. A.: Box model studies of the secondary organic aerosol formation under different HC/NO_x conditions using the subset of the Master Chemical Mechanism for α-pinene oxidation, J. Geophys. Res., 113, D10301, doi:10.1029/2007JD008726, 2008.
Yokelson, R. J., Karl, T., Artaxo, P., Blake, D. R., Christian, T. J., Griffith, D. W. T., Guenther, A.,

and Hao, W. M.: The Tropical Forest and Fire Emissions Experiment: overview and airborne fire emission factor measurements, Atmos. Chem. Phys., 7, 5175–5196, 2007, http://www.atmos-chem-phys.net/7/5175/2007/.

Yokelson, R. J., Urbanski, S. P., Atlas, E. L., Toohey, D. W., Alvarado, E. C., Crounse, J. D., Wennberg, P. O., Fisher, M. E., Wold, C. E., Campos, T. L., Adachi, K., Buseck, P. R., and Hao, W. M.: Emissions from forest fires near Mexico City, Atmos. Chem. Phys., 7, 5569–5584, 2007, http://www.atmos-chem-phys.net/7/5569/2007/.

Zhang, J., Huff Hartz, K. E., Pandis, S. N., and Donahue, N. M.: Secondary organic aerosol formation from limonene ozonolysis: Homogeneous and heterogeneous influences as a function of NO_x, J. Phys. Chem. A, 110, 11053–11063, 2006.

Zhang, Q., Alfarra, M. R., Worsnop, D. R., Allan, J. D., Coe, H., Canagaratna, M. R., and Jimenez, J. L.: Deconvolution and Quantification of Hydrocarbon-like and Oxygenated Organic Aerosols Based on Aerosol Mass Spectrometry, Environ. Sci. Technol., 39, 4938–4952, 2005.

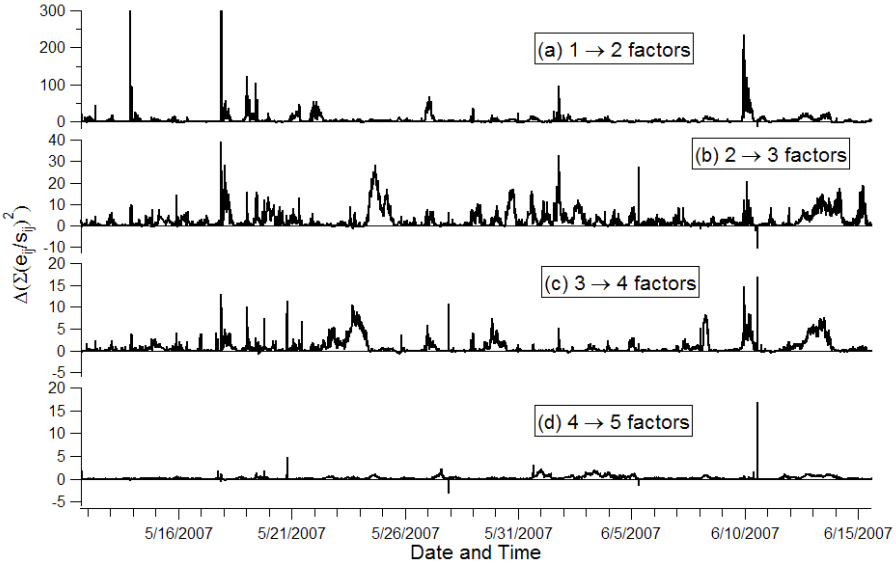

Fig. 1. Effect of the number of factors in the PMF solution on the time-dependent contribution to *Q*. The plotted quantity is the difference between the two cited solutions, i.e. Fig. 1a shows contribution to *Q* for the 1-factor solution minus that of the 2-factor solution.

ACPD
9, 18113–18158, 2009

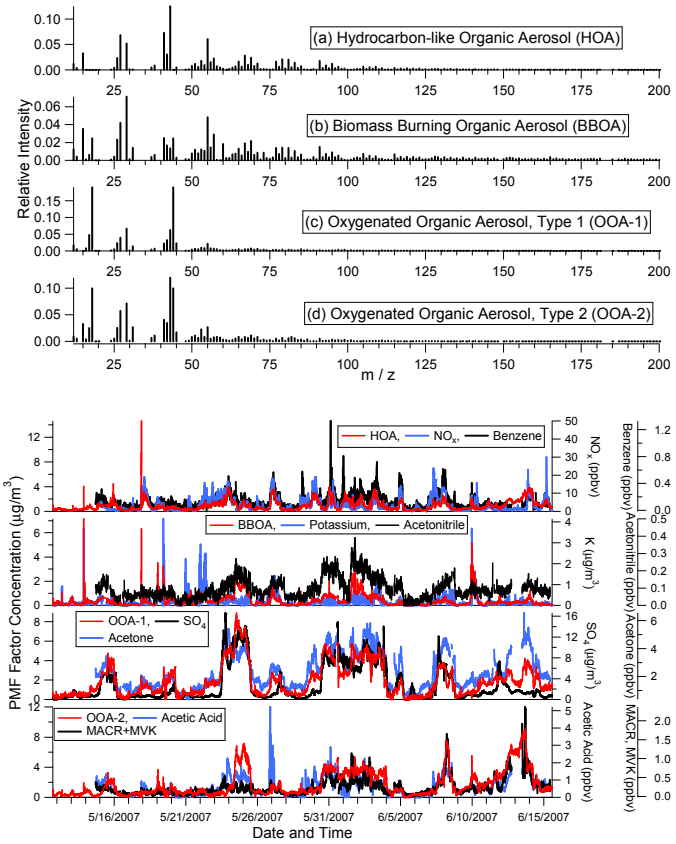

Fig. 2. Factor mass spectra **(a)** and time series **(b)** for the 4-factor solution to the AMS dataset. Mass spectra are normalized such that the sum of each spectrum across all *m/z*'s is equal to 1. Time series are plotted for both AMS PMF factors (red traces, left axis) and selected tracer species (black and blue traces, right axis).

ACPD
9, 18113–18158, 2009

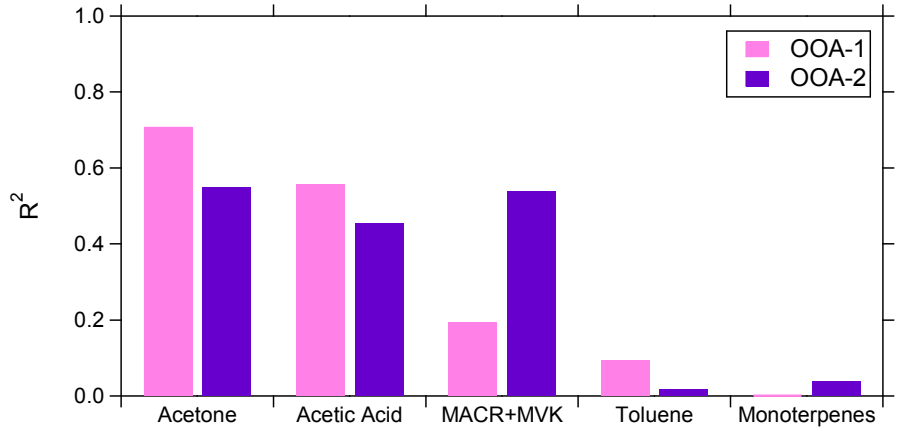

Fig. 3. Correlations between the time series of OOA-1 and OOA-2 factors with selected VOCs over the entire study period.

ACPD

9, 18113–18158, 2009

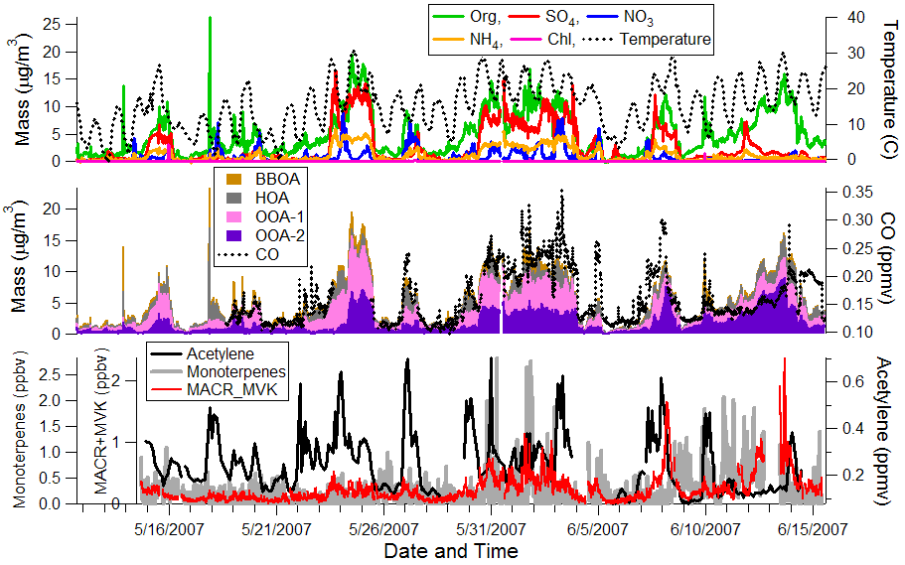

Fig. 4. Time series of AMS measurements (top panel), AMS PMF factors (middle panel), and selected gas-phase species (bottom panel). Mixing ratios of methacrolein and methyl vinyl ketone (MACR+MVK) and monoterpenes are obtained from the PTR-MS measurements at *m/z* 71 and 137, respectively. Acetylene was obtained from GC-FID measurements.

ACPD
9, 18113–18158, 2009

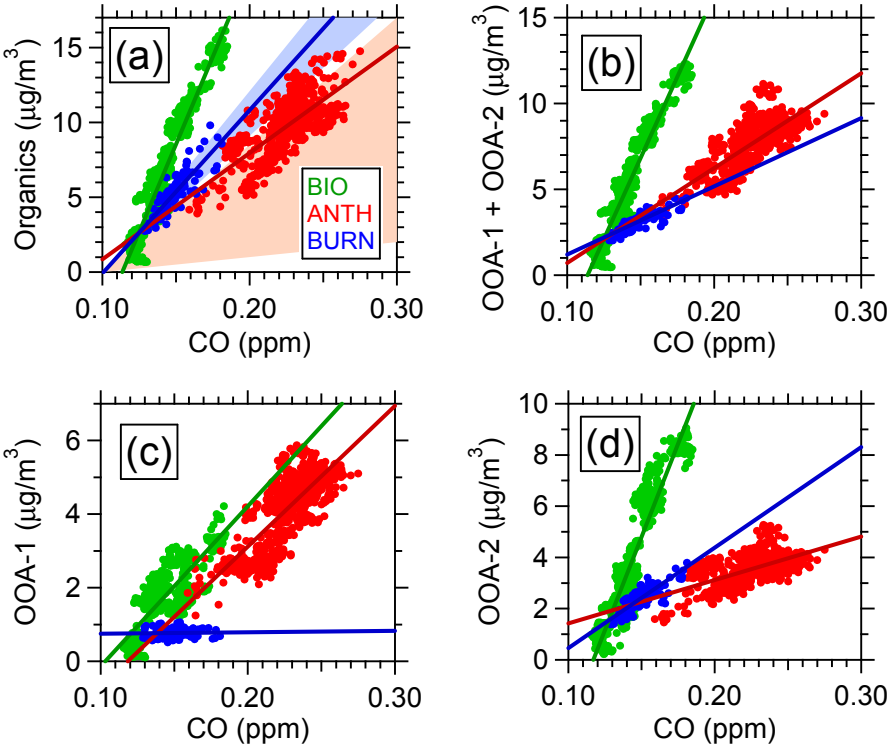

Fig. 5. Mass concentration of **(a)** total organics, **(b)** OOA-1+OOA-2, **(c)** OOA-1, and **(d)** OOA-2 as a function of CO for selected periods dominated by biogenic (green), anthropogenic (red), and biomass burning (blue) sources. The blue and red shaded regions in Fig. 5a denotes the range of previously observed values for ΔOM/ΔCO for biomass burning (Reid et al., 2005; Yokelson et al., 2007a, b) and anthropogenically-influenced regions (de Gouw et al., 2008; DeCarlo et al., 2008; Kleinman et al., 2009), respectively.

ACPD
9, 18113–18158, 2009

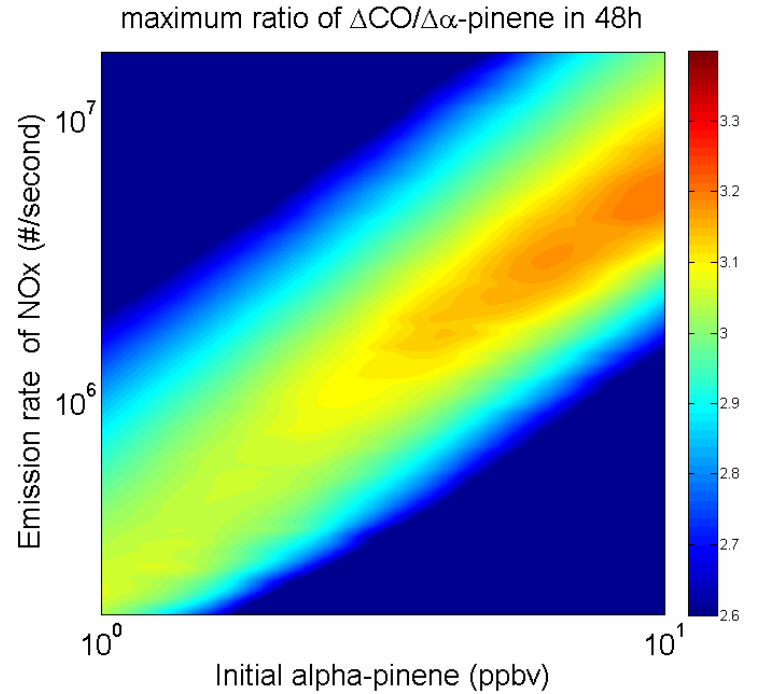

Fig. 6. Ratio of ΔCO/Δα-pinene (colors) as a function of NO_x emission rate and initial α-pinene concentration for 48 h Master Chemical Mechanism model runs.

ACPD
9, 18113–18158, 2009

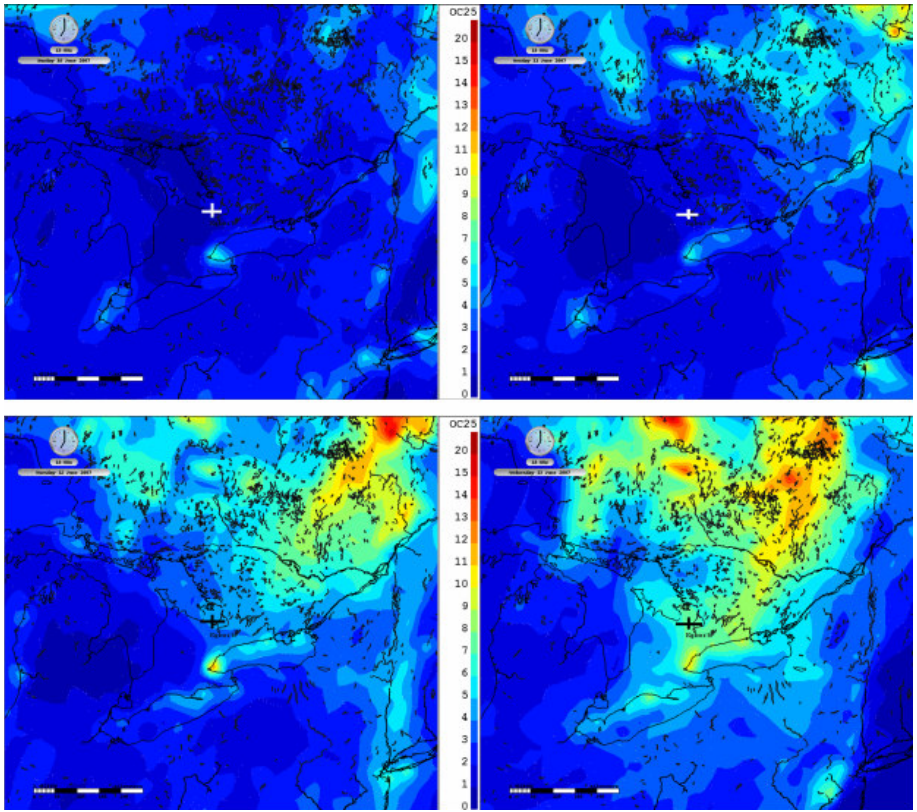

Fig. 7. Predicted $PM_{2.5}$ SOA spatial distributions for the 42 km resolution grid. Images are for 19Z on 10, 11, 12 and 13 June. A cross marks the Egbert site. The color legend represents the mass concentration of SOA in $\mu g/m^3$.

ACPD

9, 18113–18158, 2009

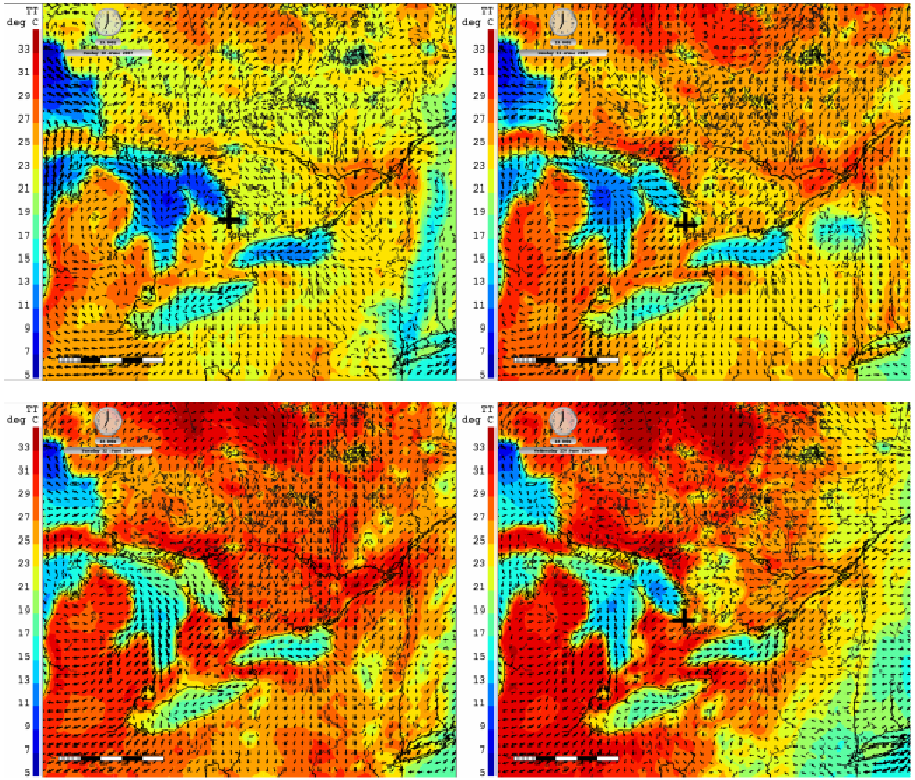

Fig. 8. Temperature and wind direction for the 15 km resolution nested grid. Images are for 19Z on 10, 11, 12 and 13 June. A cross marks the Egbert site. The color legend represents the temperature in ˚C. Arrows denote wind direction.

ACPD

9, 18113–18158, 2009

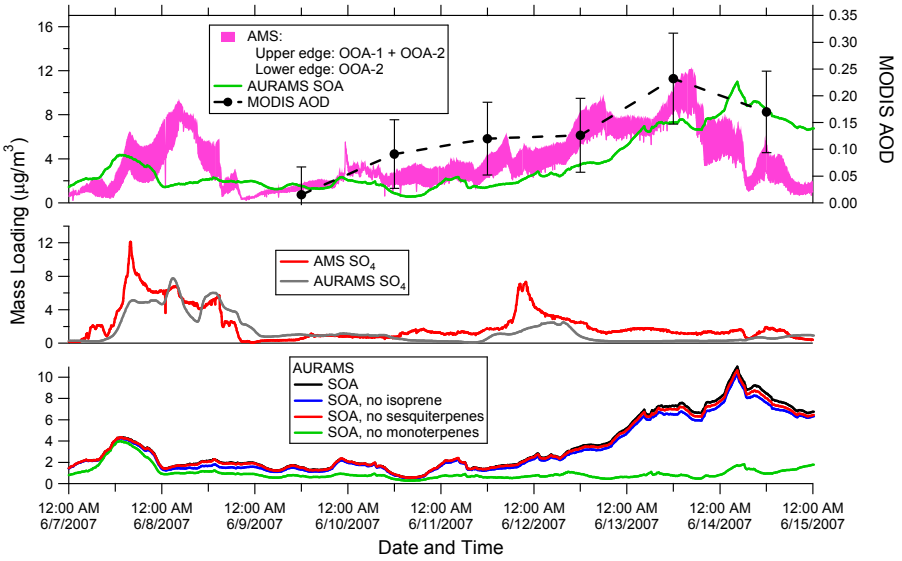

Fig. 9. Comparison of experimental measurements, AURAMS model results, and MODIS regional AOD (top 2 panels), and AURAMS sensitivity tests (bottom panel). AURAMS results are obtained from a 42 km grid in the top and bottom panels and a 15 km grid in the bottom panel. Error bars for MODIS AOD denote uncertainties in the retrieval.

ACPD
9, 18113–18158, 2009

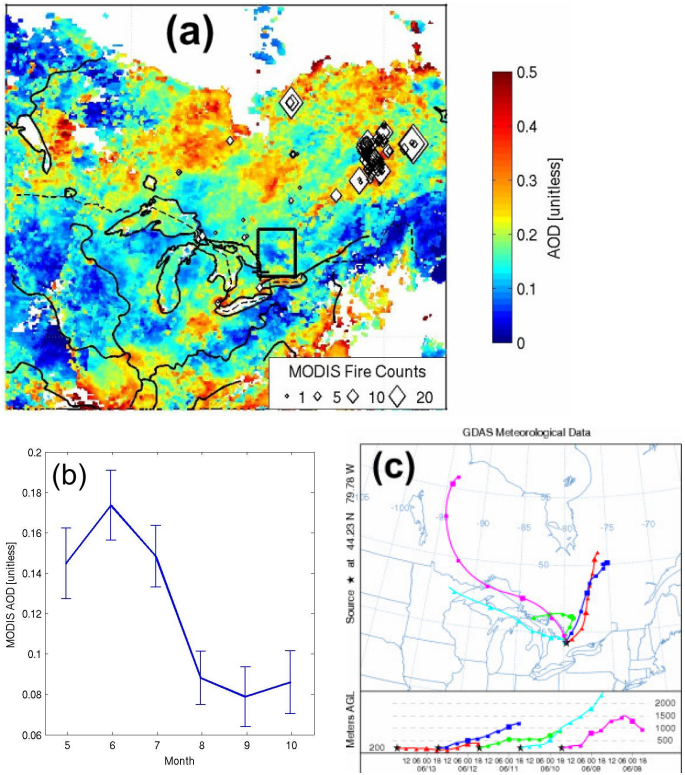

Fig. 10. (a) MODIS aerosol optical depth (colors) and fire counts (diamonds) over Ontario and Quebec during the peak of the biogenic period (12 to 14 June 2007). The sampling location is denoted as a cross; the 3° by 3° box was used to calculate regional AOD in Fig. 9. **(b)** Monthly MODIS AOD average from 2001 to 2006 calculated within the boxed region of Fig. 10a. Error bars denote uncertainties in the MODIS AOD retrieval. **(c)** 48-h back trajectories ending at the Egbert site.

ACPD
9, 18113–18158, 2009